**Author(s):** Hassan, MennaAllah; El-Faham, Ayman; Barakat, Assem; Haukka, Matti; Tatikonda, Rajendhraprasad; Abu-Youssef, Morsy A. M.; Soliman, Saied M.; Yousri, Amal

**Title:** Synthesis, X-ray Structure, Cytotoxic, and Anti-Microbial Activities of Zn(II) Complexes with a Hydrazono s-Triazine Bearing Pyridyl Arm

**Year:** 2024

**Version:** Published version



**Please cite the original version:**

Hassan, M., El-Faham, A., Barakat, A., Haukka, M., Tatikonda, R., Abu-Youssef, M. A. M., Soliman, S. M., & Yousri, A. (2024). Synthesis, X-ray Structure, Cytotoxic, and Anti-Microbial Activities of Zn(II) Complexes with a Hydrazono s-Triazine Bearing Pyridyl Arm. Inorganics, 12(7), Article 176. https://doi.org/10.3390/inorganics12070176

*inorganics*

MDPI

*Article*

# Synthesis, X-ray Structure, Cytotoxic, and Anti-Microbial Activities of Zn(II) Complexes with a Hydrazono *s*-Triazine Bearing Pyridyl Arm

**MennaAllah Hassan [1], Ayman El-Faham [1], Assem Barakat [2], Matti Haukka [3], Rajendhraprasad Tatikonda [3], Morsy A. M. Abu-Youssef [1], Saied M. Soliman [1,*] and Amal Yousri [1,*]**

[1] Department of Chemistry, Faculty of Science, Alexandria University, P.O. Box 426, Ibrahimia, Alexandria 21321, Egypt; mennaallahhassanelsayed@gmail.com (M.H.); ayman.elfaham@alexu.edu.eg or aymanel_faham@hotmail.com (A.E.-F.); morsy5@alexu.edu.eg (M.A.M.A.-Y.)

[2] Department of Chemistry, College of Science, King Saud University, P.O. Box 2455, Riyadh 11451, Saudi Arabia; ambarakat@ksu.edu.sa

[3] Department of Chemistry, University of Jyväskylä, P.O. Box 35, FI-40014 Jyväskylä, Finland; matti.o.haukka@jyu.fi (M.H.); rp.tatikonda@jyu.fi (R.T.)

* Correspondence: saied1soliman@yahoo.com or saeed.soliman@alexu.edu.eg (S.M.S.); amal.yousri@alexu.edu.eg or amalyousri@yahoo.com (A.Y.)

**Abstract:** The $[ZnL(ONO_2)_2]$ **1** and $[ZnL(NCS)_2]$ **2** complexes were synthesized using self-assembly of the *s*-triazine tridentate ligand (**L**) with $Zn(NO_3)_2{\cdot}6H_2O$ and $Zn(ClO_4)_2{\cdot}6H_2O/NH_4SCN$, respectively. The Zn(II) is further coordinated by two nitrate and two isothiocyanate groups as monodentate ligands in **1** and **2**, respectively. Both complexes have distorted square pyramidal coordination environments where the extent of distortion is found to be greater in **2** ($\tau_5$ = 0.41) than in **1** ($\tau_5$ = 0.28). Hirshfeld calculations explored the significant C···O, C···C, N···H, and O···H contacts in the molecular packing of both complexes. The energy framework analysis gave the total interaction energies of −317.8 and −353.5 kJ/mol for a single molecule in a 3.8 Å cluster of **1** and **2**, respectively. The total energy diagrams exhibited a strong resemblance to the dispersion energy frameworks in both complexes. NBO charge analysis predicted the charges of the Zn(II) in complexes **1** and **2** to be 1.217 and 1.145 e, respectively. The electronic configuration of Zn1 is predicted to be [core] $4S^{0.32}$ $3d^{9.98}$ $4p^{0.45}$ $4d^{0.02}$ $5p^{0.01}$ for **1** and [core] $4S^{0.34}$ $3d^{9.97}$ $4p^{0.53}$ $4d^{0.02}$ for **2**. The increased occupancy of the valence orbitals is attributed to the donor→acceptor interactions from the ligand groups to Zn(II). The Zn(II) complexes were examined for their cytotoxic and antimicrobial activities. Both **1** and **2** have good cytotoxic efficiency towards HCT-116 and A-549 cancerous cell lines. We found that **1** is more active ($IC_{50}$ = 29.53 ± 1.24 and 35.55 ± 1.69 μg/mL) than **2** ($IC_{50}$ = 41.25 ± 2.91 and 55.05 ± 2.87 μg/mL) against both cell lines. Also, the selectivity indices for the Zn(II) complexes are higher than one, indicating their suitability for use as anticancer agents. In addition, both complexes have broad-spectrum antimicrobial activity ($IC_{50}$ = 78–625 μg/mL) where the best result is found for **2** against *P. vulgaris* ($IC_{50}$ = 78 μg/mL). Its antibacterial activity is found to be good compared to gentamycin (5 μg/mL) as a positive control against this microbe.

**Keywords:** *s*-Triazine; Zn(II); X-ray structure; energy framework; NBO; cytotoxicity; antimicrobial

check for updates

**Citation:** Hassan, M.; El-Faham, A.; Barakat, A.; Haukka, M.; Tatikonda, R.; Abu-Youssef, M.A.M.; Soliman, S.M.; Yousri, A. Synthesis, X-ray Structure, Cytotoxic, and Anti-Microbial Activities of Zn(II) Complexes with a Hydrazono *s*-Triazine Bearing Pyridyl Arm. *Inorganics* **2024**, *12*, 176. https://doi.org/10.3390/inorganics12070176

Academic Editor: Marius Andruh

Received: 5 June 2024
Revised: 15 June 2024
Accepted: 19 June 2024
Published: 21 June 2024



## 1. Introduction

There is no doubt about the significant role of zinc in biology as it is ranked the second most common trace metal in our bodies [1]. Also, it is included in several enzymes as a catalyst and/or co-catalyst [2–5]. In cellular processes, zinc is primarily linked to N, O, or S-atoms of protein residues [6] where insufficient levels of zinc are found related to cancer growth for both humans and animals [7,8]. Several zinc complexes have interesting applications in biology [9–23]. For example, Zn(II) complexes of 3-nitro-4-hydroxybenzoic acid were reported to have anticonvulsant activity [9]. Additionally, Zn(II)

complexes with amino acids such as [Zn(L-Asn)$_2$], [Zn(L-Pro)$_2$], [Zn(L-Thr)$_2$], and [Zn(L-Val)$_2$] have interesting insulin-mimetic activity which is found to be dependant on their overall stability constants [10]. In addition, Zn(II)-Indomethacin complexes were patented as veterinary pharmaceutics having anti-inflammatory properties [11]. Furthermore, their in vitro antioxidant and inhibition properties versus soybean lipoxygenase were found to be promising [18]. It is found that the Zn(II)-mefenamic acid (Hmef) complexes have higher antioxidant activity than the free Hmef where the [Zn(mefenamic acid)$_2$($H_2O$)$_4$] complex has the highest scavenging activity. A few of the numerous biological actions associated with zinc complexes are their interesting antibacterial [12–17] and antitumor [20–22] properties. Also, it is beneficial in reducing the hepato-toxicity that arises from some anticancer drugs [24]. Its low toxicity compared to other metal-based medications is one of the most important medicinal properties of zinc complexes.

On the other hand, the development of new materials with interesting biological properties [25–28] as antimicrobial and anticancer agents is a challenge for researchers working in this field. Among the most promising organic scaffolds, *s*-triazine derivatives attracted the attention of chemists due to their low cost and ease of preparation, in addition to their structural and biological diversities. Their activities include antiplasmodial effects [25], antibacterial properties [26], anticancer potential [27], and function as carbonic anhydrase inhibitors [28]. Also, they are considered as interesting multidentate ligands that are important not only for the construction of a diverse range of supramolecular structures but also for creating functional supplies for a lot of applications [29–32]. Many of the *s*-triazine multidentate ligands play a significant role in inorganic chemistry. Interestingly, little changes in the substituents attached to *s*-triazine altering their steric and electronic properties affect their reactivity towards different metal ions [33].

In this work, an exploration of the structural properties of two Zn(II) complexes with the *s*-triazine ligand (**L**) shown in Figure 1 is presented. The new complexes were synthesized using a self-assembly technique and characterized using elemental analysis, FTIR, $^1$H NMR (for complex **1**) spectra, and X-ray diffraction from a single crystal. The antibacterial and cytotoxic properties of the new compounds were also investigated. Additionally, NBO calculations were employed to elucidate the different coordination interactions that occurred between Zn(II) and the donor atoms coordinating it [34,35].

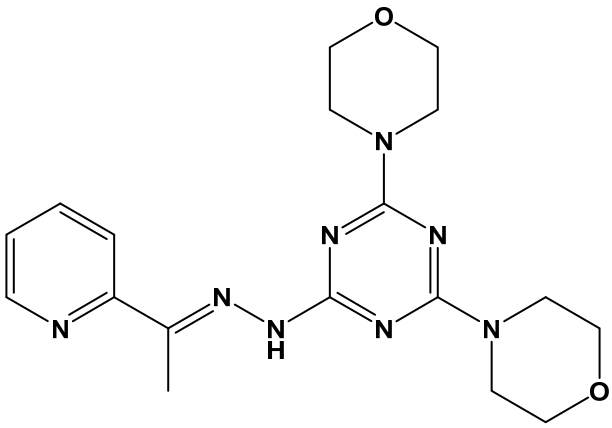


**2,4-*Bis*(morpholin-4-yl)-6-[(*E*)-2-[1- (pyridin-2-yl)ethylidene]hydrazin-1-yl]-1,3,5-triazine**

**Figure 1.** Structure of **L** [34,35].

## 2. Results and Discussion

### *2.1. Synthesis and Characterizations*

The reaction of **L** with $Zn(NO_3)_2{\cdot}6H_2O$ or $Zn(ClO_4)_2.6H_2O/NH_4SCN$ in ethanol yielded the heteroleptic complexes, [ZnL($ONO_2$)$_2$] (**1**) and [ZnL(NCS)$_2$] (**2**), respectively (Scheme 1). The FTIR spectra of **1** and **2** (Figures S1 and S2; Supplementary Data) exhibit distinct spectral bands for the $\nu_{(C=N)}$ vibrations at 1579 and 1588 cm$^{-1}$, respectively, while

for **L** this band appeared at 1584 $cm^{-1}$. The $\nu_{(C=C)}$ vibration appeared at 1513, 1502, and 1492 $cm^{-1}$ in the FTIR spectra of **1**, **2**, and **L**, respectively. These shifts are attributed to the complexation between Zn(II) and **L**. A new sharp band appeared at 1391 $cm^{-1}$ only in **1** but did not appear in the free ligand, which is attributed to the $\nu_{(N-O)}$ mode of the $NO_3^-$ group. Also, the double split sharp band that appeared at 2047 and 2084 $cm^{-1}$ is assigned to the $\nu_{(SCN)}$ vibrations in **2**.

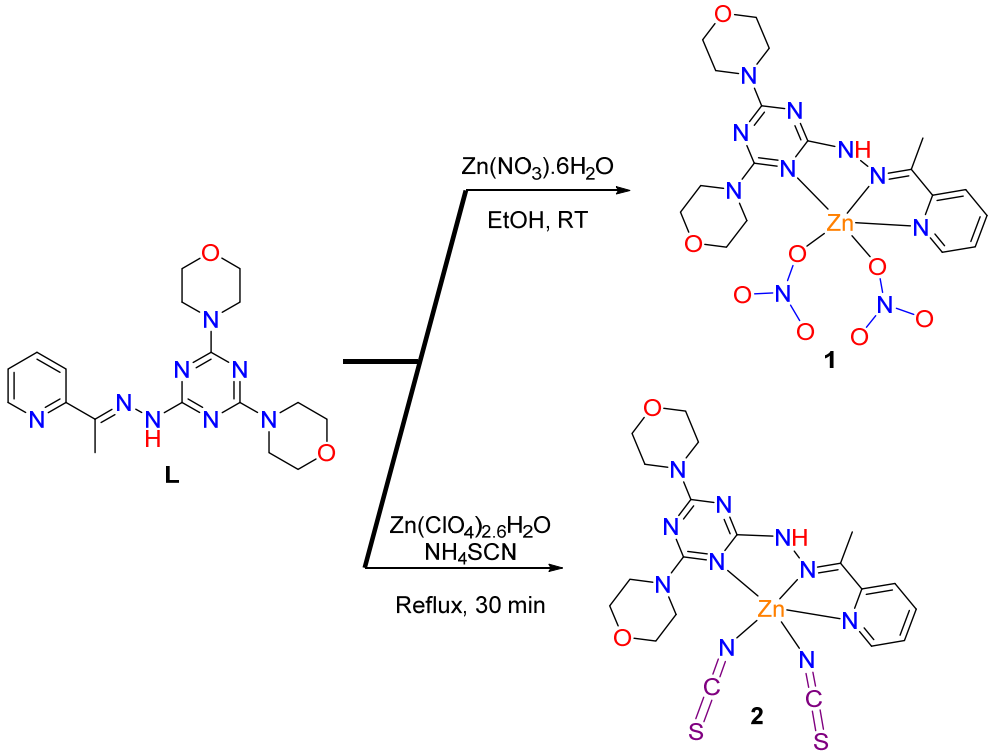


**Scheme 1.** Syntheses of **1** and **2**.

In addition, the $^1$H NMR spectra of complex **1** are recorded in DMSO as solvent (Figure S3; Supplementary data). The $^1$H NMR spectra showed the methyl group as a singlet at δ 2.33 ppm, while the free ligand appeared at δ 2.40 ppm [34]. Also, the protons of the morpholine moiety in complex **1** appeared as two broad singlet peaks at δ 3.71 ($CH_2$-O-$CH_2$) and 3.59 ppm ($CH_2$-N-$CH_2$) compared to δ 3.81 and 3.72 ppm for **L**, respectively. The hydrogens of the pyridyl moiety showed reasonable shifts at δ 8.53, 8.06, 7.78, and 7.31 ppm compared to δ 8.20, 8.08, 7.67, and 7.20 ppm in the free **L**, respectively. Also, the NH of complex **1** showed a reasonable shift as a broad singlet peak at δ 9.72 compared δ to 8.54 ppm for the NH of the free **L**. The $^1$H NMR spectral analysis of complex **1** confirmed the coordination of Zn(II) with **L** in solution. Furthermore, the structure of both complexes was confirmed using X-ray single crystal diffraction (SCXRD).

### 2.2. *X-ray Structure Description for* [ZnL($ONO_2$)$_2$]; **1**

The structure of **1** was verified through X-ray crystallography revealing the monomeric formula [ZnL($ONO_2$)$_2$] (Figure 2). Its crystal system is orthorhombic and its space group is $P2_12_12_1$. The cell dimensions are $a$ = 7.92330(10), $b$ = 11.89480(10), and $c$ = 24.3806(2) Å, while the number of molecules in the unit cell is four and crystal density is 1.659 g·$cm^{-3}$ (Table 1).

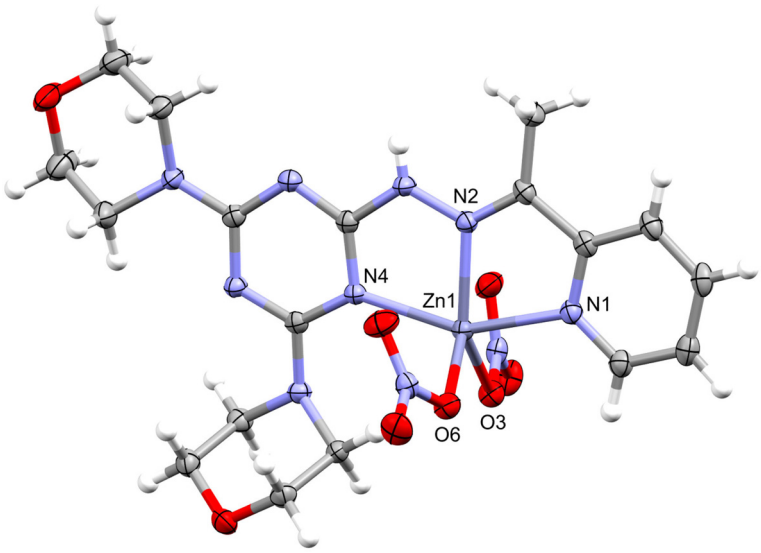


**Figure 2.** X-ray structure showing atom numbering for **1**.

**Table 1.** Crystal data for **1** and **2**.

| | **[ZnL(ONO$_2$)$_2$]; (1)** | **[ZnL(NCS)$_2$]; (2)** |
|---|---|---|
| CCDC | 2359261 | 2359262 |
| Empirical formula | $C_{18}H_{24}N_{10}O_8Zn$ | $C_{20}H_{24}N_{10}O_2S_2Zn$ |
| Fw | 573.84 | 565.98 |
| Temp (K) | 120.00(10) | 120.00(10) |
| $\lambda$ (Å) | 1.54184 | 1.54184 |
| Cryst syst | Orthorhombic | Monoclinic |
| Space group | $P2_12_12_1$ | $P2_1/c$ |
| $a$ (Å) | 7.92330(10) | 13.8914(2) |
| $b$ (Å) | 11.89480(10) | 20.5446(2) |
| $c$ (Å) | 24.3806(2) | 8.97020(10) |
| β (deg) | 90 | 108.195(2) |
| $V$ (Å$^3$) | 2297.78(4) | 2432.03(6) |
| Z | 4 | 4 |
| $\rho_{calc}$ (Mg/m$^3$) | 1.659 | 1.546 |
| $\mu$ (Mo K$\alpha$) (mm$^{-1}$) | 2.104 | 3.352 |
| No. reflns. | 25,015 | 25,012 |
| Unique reflns. | 4934 | 5007 |
| Completeness to θ = 67.684° | 100% | 99.6% |
| Absolute structure parameter | −0.020(6) | |
| GOOF (F$^2$) | 1.057 | 1.041 |
| $R_{int}$ | 0.0274 | 0.0246 |
| $R_1$ [a] ($I \geq 2\sigma$) | 0.0220 | 0.0301 |
| $wR_2$ [b] ($I \geq 2\sigma$) | 0.0587 | 0.0722 |

[a] $R_1 = \Sigma||F_o| - |F_c||/\Sigma|F_o|$. [b] $wR_2 = \{\Sigma[w(F_o^2 - F_c^2)^2]/\Sigma[w(F_o^2)^2]\}^{1/2}$.

The structure of this complex showed one [ZnL(ONO$_2$)$_2$] molecule as a symmetric formula. In this neutral complex, the Zn(II) is penta-coordinated with three nitrogen atoms from the *s*-triazine ligand (**L**). There are three different Zn-N interactions where the Zn-N$_{(hydrazone)}$ is the shortest (Zn1-N2; 2.0443(19) Å) while the Zn-N$_{(s\text{-triazine})}$ is the longest (Zn1-N4; 2.1713(19) Å) (Table 2). The same trend was found in the structurally related Mn(II) and Cu(II) complexes of the same ligand (**L**) [34]. In addition, there are two Zn-O coordination interactions belonging to two monodentate nitrate groups, which are different in their distances. The Zn1-O3 and Zn1-O6 distances are 2.0448(16) and 2.0131(17) Å, respectively, while the angle O6-Zn1-O3 is 100.30(7)°. Hence, the structure of the $ZnN_3O_2$ coordination sphere could be described as a highly distorted penta-coordinated system.

The $\tau_5$ parameter is calculated to be 0.28, indicating a distorted penta-coordinated system that is close to square pyramidal geometry [36]. The same distorted penta-coordination environment was observed in case of the Mn(II) and Cu(II) complexes where the $\tau_5$ values were calculated to be 0.33 and 0.24, respectively [34]. Hence, the square pyramidal configuration showed the lowest distortion in case of the Cu(II) complex. In addition, the coordination mode of nitrate groups in this complex is described using Equation (1). The $\gamma$ values for the $N(9)O_3^-$ and $N(10)O_3^-$ groups are 0.90 and 0.86, indicating terminally coordinated monodentate nitrate groups [37,38].

$$\gamma = \frac{(d_1 - d_2)}{\Delta} \quad (1)$$

where the order of N-O distances ($d$) is $d_1 \geq d_2 \geq d_3$ and $\Delta = d_1 - d_3$.

**Table 2.** Important bond lengths (Å) and angles (°) for **1**.

| Bond Length | | | |
|---|---|---|---|
| Zn1-O3 | 2.0448(16) | Zn(1)-N(2) | 2.0443(19) |
| Zn1-O6 | 2.0131(17) | Zn(1)-N(4) | 2.1713(19) |
| Zn1-N1 | 2.1416(19) | | |
| **Bond Angle** | | | |
| O3-Zn1-N1 | 94.98(7) | O(6)-Zn(1)-N(4) | 105.96(7) |
| O3-Zn1-N4 | 101.93(7) | N(1)-Zn(1)-N(4) | 153.23(7) |
| O6-Zn1-O3 | 100.30(7) | N(2)-Zn(1)-O(3) | 136.51(7) |
| O6-Zn1-N1 | 91.02(8) | N(2)-Zn(1)-N(1) | 75.36(8) |
| O6-Zn1-N2 | 121.80(7) | N(2)-Zn(1)-N(4) | 78.09(7) |

The molecular packing of the $[ZnL(ONO_2)_2]$ complex showed two types of non-covalent interactions (Table 3). The presentation of these hydrogen bond contacts is shown in Figure 3A. There is one significant N-H···O hydrogen bond, which occurred between the hydrazone N-H as the hydrogen bond donor and the O atoms from the nitrate ion as the acceptor for a hydrogen bond. The hydrogen to acceptor distance is 2.15(3) Å for N3-H3···O5 while the donor to acceptor distance is 2.915(3) Å. Furthermore, there are many C-H···O interactions that occurred with the O atoms of the $NO_3^-$ group as the H-bond acceptor where the hydrogen to acceptor (O) distances range from 2.36 Å (C1-H1···O4) to 2.57 Å (C2-H2···O7) while the donor (C) to acceptor (O) distances range from 3.109(3) Å (C1-H1···O4) to 3.495(3) Å (C7-H7C···O5), respectively. The resulting packing scheme is shown in Figure 3B. Thus, the packing of **1** could be illustrated as a network of hydrogen bonds extended along the *a*-axis.

**Table 3.** Hydrogen bonds for **1** (Å and °).

| D-H···A | d(D-H) | d(H···A) | d(D···A) | D-H···A |
|---|---|---|---|---|
| N3-H3···O5 [a] | 0.79(3) | 2.15(3) | 2.915(3) | 164(3) |
| C1-H1···O4 [b] | 0.95 | 2.36 | 3.109(3) | 135 |
| C2-H2···O7 [c] | 0.95 | 2.57 | 3.260(3) | 130 |
| C7-H7C···O5 [a] | 0.98 | 2.56 | 3.495(3) | 160′ |
| C11-H11A···O8 [d] | 0.99 | 2.53 | 3.216(3) | 127 |
| C13-H13A···O6 [e] | 0.99 | 2.48 | 3.460(3) | 171 |
| C14-H14A···O4 [a] | 0.99 | 2.50 | 3.372(3) | 147 |
| C17-H17A···O1 [f] | 0.99 | 2.49 | 3.327(3) | 142 |

[a] 1 − x,1/2 + y,3/2 − z; [b] 1 − x,−1/2 + y,3/2 − z; [c] −x,−1/2 + y,3/2 − z; [d] 1/2 + x,1/2 − y,1 − z; [e] x,1 + y,z; [f] x,−1 + y,z.

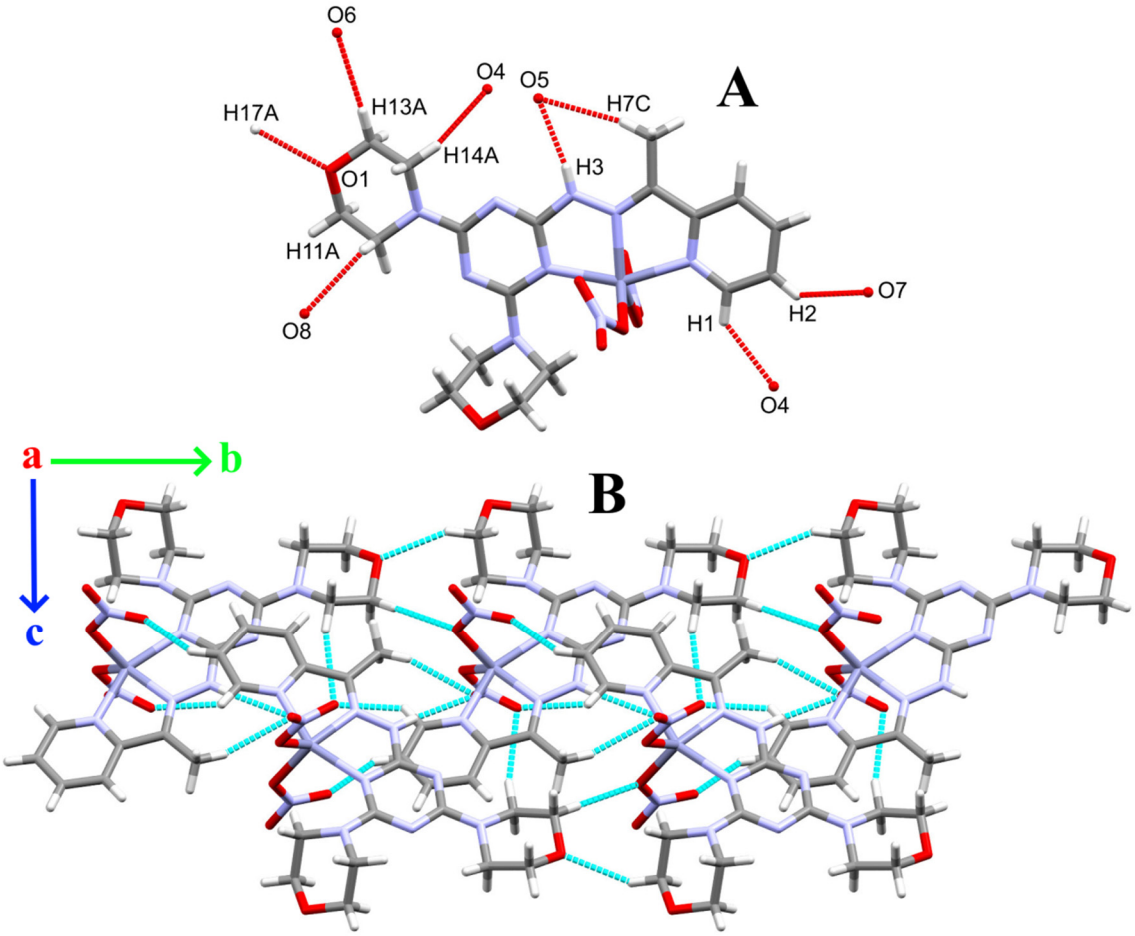


**Figure 3.** The important H-bond contacts (**A**) and the packing scheme (**B**) for **1** along the *a*-axis.

Aromatic–aromatic interactions are significant non-covalent intermolecular forces that are akin to hydrogen bonding in importance. The X-ray structure analysis revealed the existence of one π–π interaction between the pyridine and *s*-triazine π-systems (Figure 4A). The C2···C9 distance is 3.237(3) Å while the ring centroids distance is 3.698 Å and the tilt angles are ranging from 20.69 to 21.95° [39]. In addition, the presence of anion–π interaction between the coordinated oxygens from the nitrate group and the π systems of pyridine is evident. There are two anion–π interactions, which are different in their distances. The O5···C5$_{(pyridine)}$ and O4···C1$_{(pyridine)}$ distances are 3.099(3) and 3.109(3) Å, respectively (Figure 4B). Also, there are some C-H···π contacts between the C16-H16B of the morpholine ring and the *s*-triazine π system where the C10···H16B, C9···H16B, and N5···H16B distances are 2.807, 2.816, and 2.628 Å, respectively (Figure 4C).

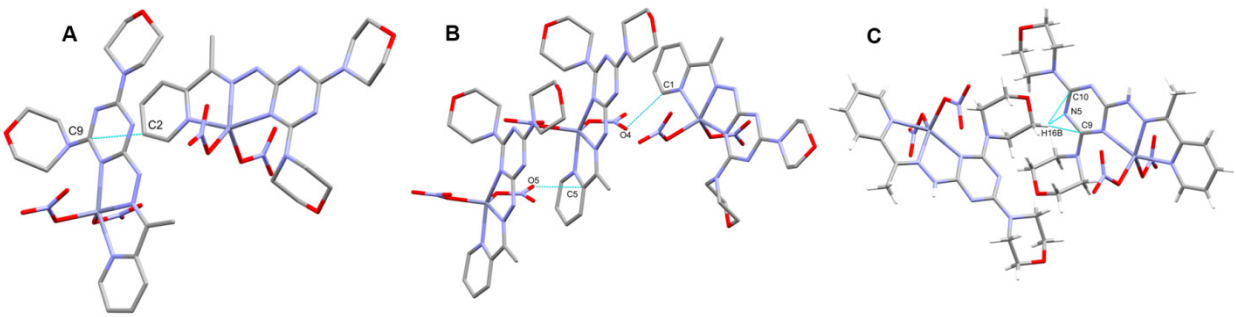


**Figure 4.** The π–π (**A**), anion–π (**B**), and C-H···π (**C**) interactions in **1**.

### 2.3. X-ray Structure Description for [ZnL(NCS)$_2$]; **2**

The synthetic procedure of **2** involved the use of $NH_4SCN$ in order to examine the coordination mode of the $SCN^-$ group. This small anion could be terminally coordinated via its N or S atoms. Also, it could bridge metal centers, leading to polynuclear metal complexes. The structure of **2** also comprised the monomeric neutral formula, [ZnL(NCS)$_2$] (Figure 5). It crystallized in the monoclinic crystal system and $P2_1/c$ space group. The unit cell parameters are $a$ = 13.8914(2), $b$ = 20.5446(2), $c$ = 8.97020(10) Å, and $\beta$ = 108.195(2)°. The number of molecules in the unit cell is four and the crystal density is 1.546 g·cm$^{-3}$ (Table 1).

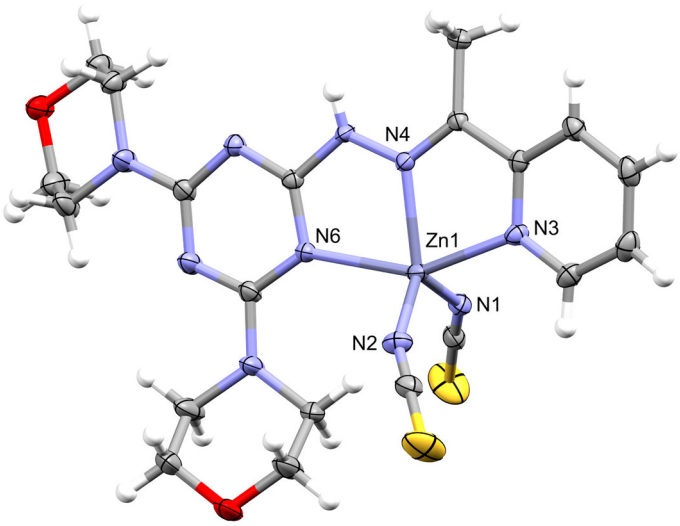


**Figure 5.** X-ray structure showing atom numbering for **2**.

Similarly, the [ZnL(NCS)$_2$] complex has five coordinated Zn(II) in which there are five different Zn-N interactions. There are three Zn-N bonds with the organic ligand **L** in addition to two Zn-N bonds with the two isothiocyanate groups. The Zn1-N1 (1.9645(15) Å) and Zn1-N2 (1.9466(16) Å) with the anionic $NCS^-$ groups are the shortest while the Zn1-N6 belonging to the *s*-triazine is longer (2.2696(14) Å) than any of the two Zn-N$_{(pyridine)}$ and Zn-N$_{(hydrazone)}$ bonds. Hence, the same order of the Zn-N distances for **L** is found in complexes **1** and **2** (Table 4). The bite angles of **L** are 76.18(5)° and 75.17(5)° for N4-Zn1-N6 and N4-Zn1-N3, respectively. In addition, the N1-Zn1-N2 angle is 120.51(6)°. As a result, the structure of the $ZnN_5$ coordination sphere could be described as a highly distorted penta-coordinated system ($\tau_5$ = 0.41). Hence, the coordination geometry of **2** is intermediate between the two ideal extremes (trigonal bipyramidal and square pyramidal) [36].

**Table 4.** Important bond lengths (Å) and angles (°) for **2**.

| **Bond Length** | | | |
|---|---|---|---|
| Zn1-N4 | 2.0565(14) | Zn1-N3 | 2.1813(14) |
| Zn1-N6 | 2.2696(14) | Zn1-N2 | 1.9466(16) |
| Zn1-N1 | 1.9645(15) | | |
| **Bond Angle** | | | |
| N4-Zn1-N6 | 76.18(5) | N3-Zn1-N6 | 151.30(5) |
| N4-Zn1-N3 | 75.17(5) | N2-Zn1-N4 | 126.46(6) |
| N1-Zn1-N4 | 112.89(6) | N2-Zn1-N6 | 103.14(6) |
| N1-Zn1-N6 | 93.43(6) | N2-Zn1-N1 | 120.51(6) |
| N1-Zn1-N3 | 99.10(6) | N2-Zn1-N3 | 92.58(6) |

The packing of **2** is controlled by the N-H···N and C-H···O non-covalent interactions shown in Figure 6. The significant N5-H5···N1 hydrogen bond occurred between the hydrazone N-H as a hydrogen bond donor and the N-atom from the isothiocyanate as

a hydrogen bond acceptor (Figure 6B). The hydrogen to acceptor distance is 2.24(3) Å while the donor to acceptor distance is 3.008(2) Å. In addition, the C5-H5A···O1 and C14-H14A···O2 interactions have donor-to-acceptor distances of 3.177(2) and 3.371(2) Å, respectively, while the H···O distances are 2.50(3) and 2.38 Å, respectively (Table 5). The resulting packing scheme is shown in Figure 6A. Therefore, the packing of **2** could be assigned as a network of hydrogen bonds extended along the *c*-axis.

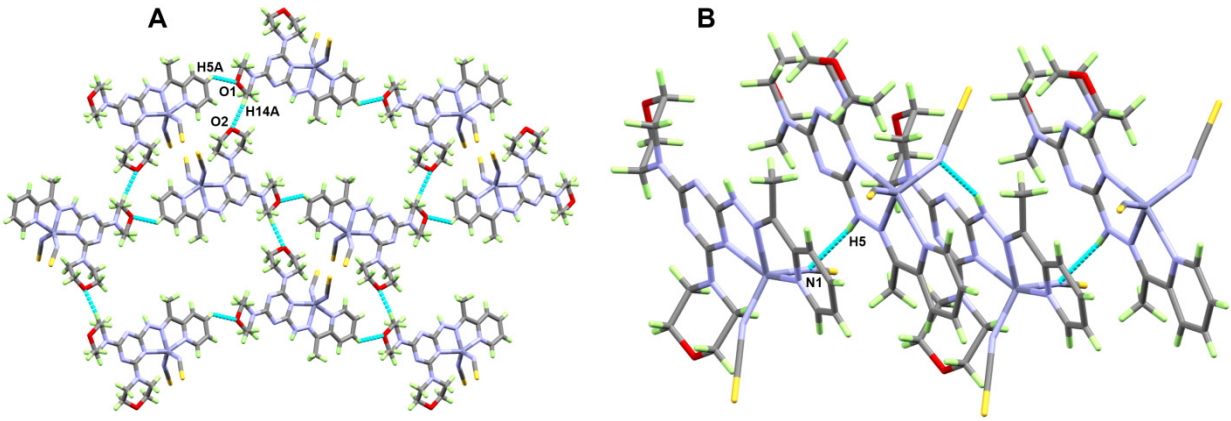


**Figure 6.** The packing schemes via O···H (**A**) and N···H (**B**) interactions in **2** along the *c*-axis.

**Table 5.** Hydrogen bonds for **2** (Å and °).

| D-H···A | d(D-H) | d(H···A) | d(D···A) | D-H···A |
|---|---|---|---|---|
| N5-H5···N1 [a] | 0.81(2) | 2.24(3) | 3.008(2) | 159(2) |
| C5-H5A···O1 [b] | 0.91(3) | 2.50(3) | 3.177(2) | 131(2) |
| C14-H14A···O2 [c] | 0.99 | 2.38 | 3.371(2) | 174 |

[a] x,1/2 − y,1/2+z; [b] −1+x,1/2 − y,−3/2+z; [c] 1 − x,−1/2+y,3/2 − z.

### *2.4. Hirshfeld Analysis*

The arrangement of molecules within a crystal has a unique pattern. The non-covalent contacts that control this organization could be analyzed using Hirshfeld calculations. For **1**, the $d_{norm}$ map and fingerprint plots of the important contacts as well as the percentages of all possible contacts along with their percentages are presented in Figure 7. Hence, the significant interactions are O···H (A), N···H (B), C···O (C), C···H (D), and C···C (E). Their percentages are 39.9, 6.0, 1.6, 8.0, and 1.2%, respectively. The fingerprint plots of all these contacts are characterized by sharp spikes and wings revealing their importance. Many O···H contacts were noted in this crystal structure where the H···O distances range from 1.940 Å (O5···H3) to 2.596 Å (O2···H3A). The short C5···O5 contact (3.099 Å) belongs to an anion–π stacking interaction between the coordinated nitrate and the pyridine moiety. On the other hand, the short C9···H16B (2.724 Å) and C10···H16B (2.741 Å) contacts refer to the C-$H_{(methyl)}$···$\pi_{(s\text{-triazine})}$ interactions. The existence of weak π–π interaction [39] between the *s*-triazine and pyridine moieties is evident from the relatively short C9···C2 (3.327 Å) contact. Also, the relatively long N5···H16B (2.549 Å) contact indicates the presence of a weak C-$H_{(morpholie)}$···$N_{(s\text{-triazine})}$ interaction. All these close contacts are depicted in Table 6.

In the case of **2**, five important non-covalent interactions were detected. The O···H (**A**), N···H (**B**), C···N (**C**), S···S (**D**), and C···H (**E**) are indicated from the corresponding fingerprint plots and $d_{norm}$ map (Figure 8). The O2···H14A (2.292 Å) and O1···H5A (2.392 Å) belong to the non-classical C-H···O interactions between the morpholine O atom and the C-H groups of the morpholine and pyridyl moieties from neighboring molecules, respectively. The other short contacts N1···H5 (2.054 Å), C1···H5 (2.501 Å), S1···S1 (3.191 Å), and C6···N2 (3.185 Å) are related to the coordinated isothiocyanate groups.

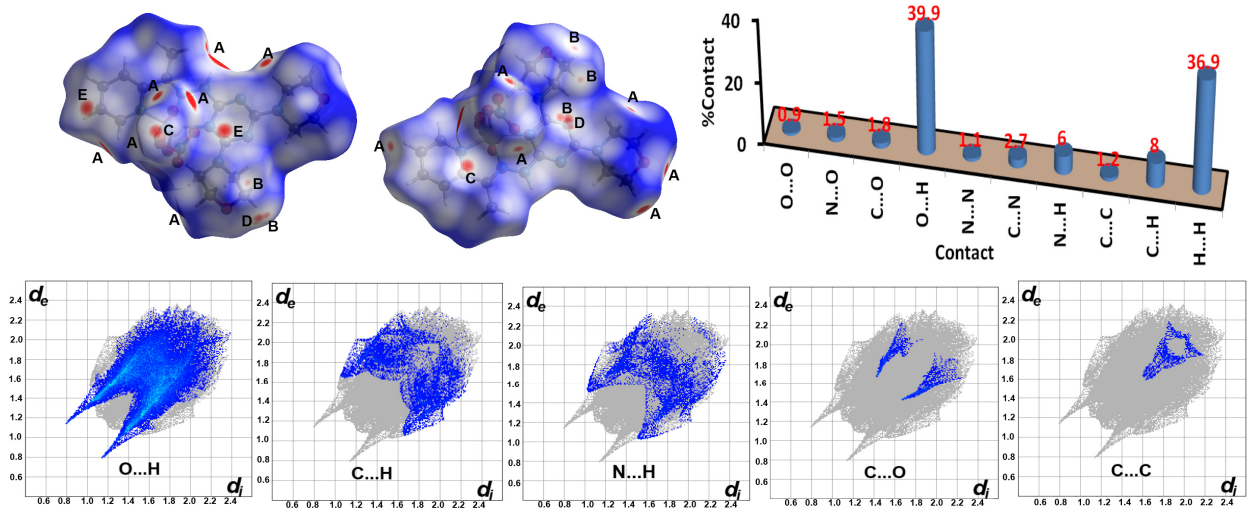


**Figure 7.** Hirshfeld surface analysis for **1**; O⋯H (A), N⋯H (B), C⋯O (C), C⋯H (D), and C⋯C (E). The shape index and curvedness maps of **1** are presented in Figure S3 (Supplementary Data).

**Table 6.** Interaction distances for close contacts in **1**.

| Interaction | Distance | Interaction | Distance |
|---|---|---|---|
| O1⋯H17A | 2.416 | C5⋯O5 | 3.099 |
| O6⋯H13A | 2.386 | C15⋯H16A | 2.747 |
| O5⋯H7C | 2.460 | C9⋯H16B | 2.724 |
| O4⋯H14A | 2.424 | C10⋯H16B | 2.741 |
| O5⋯H3 | 1.940 | C16⋯H13A | 2.739 |
| O4⋯H1 | 2.266 | N5⋯H16B | 2.549 |
| O7⋯H2 | 2.486 | C9⋯C2 | 3.327 |
| O8⋯H11A | 2.472 | | |
| O2⋯H3A | 2.596 | | |

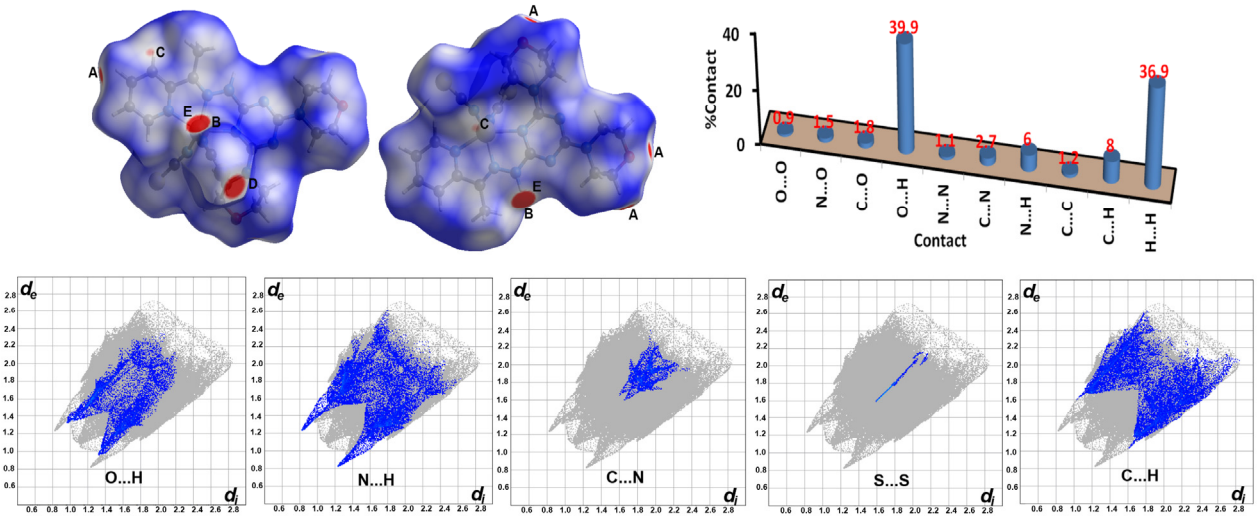


**Figure 8.** Hirshfeld surface analysis for **2**; O⋯H (A), N⋯H (B), C⋯N (C), S⋯S (D), and C⋯H (E). The other maps of **2** are presented in Figure S4 (Supplementary Data).

### *2.5. Energy Framework Analysis*

The energy framework (EFW) study is a valuable method used to analyze the topology of molecular interactions within a crystal [40–51]. Visualization of molecular interactions within a cluster with a radius of 3.8 Å between the central molecule under investigation and

its neighboring molecules for **1** and **2** is shown in Figure S5 (Supplementary Data). An energy breakdown for the intermolecular interactions that occurred in **1** is depicted in Table S1 (Supplementary Data). The total interaction energy ($E_{tot}$) is calculated to be −317.8 kJ/mol involving the electrostatic ($E_{ele}$ = −162.8 kJ/mol), polarization ($E_{pol}$ = −52.1 kJ/mol), dispersion ($E_{dis}$ = −225.9 kJ/mol), and repulsion ($E_{rep}$ = 123.0 kJ/mol) interaction energies. For **2**, the $E_{tot}$ is calculated to be −353.5 kJ/mol involving $E_{ele}$, $E_{pol}$, $E_{dis}$, and $E_{rep}$ of −147.9, −66.5, −279.0, and 139.7 kJ/mol, respectively (Table S2; Supplementary Data). In addition, the interactions between the central molecule and the −x, y+1/2, −z+1/2 symmetry molecule (light blue) for **1** and the x, −y+1/2, z+1/2 symmetry molecule (red) for **2** are the strongest. The $E_{tot}$ values are −112.8 and −143.8 kJ/mol, respectively, while their $E_{ele}$, $E_{pol}$, $E_{dis}$, and $E_{rep}$ values are −70.3, −26.5, −89.5, and 95.7 kJ/mol for **1** and −70.0, −32.4, −126.1, and 103.7 kJ/mol for **2**, respectively. The next stronger interactions are the −x, y+1/2, −z+1/2 symmetry molecule (yellow; −60.0 kJ/mol) and −x, −y, −z symmetry molecule (purple; −77.6 kJ/mol) for **1** and **2**, respectively. The total energy diagrams exhibited a strong resemblance to the dispersion energy frameworks in the two complexes, indicating the significant contribution of dispersion forces to the total forces in crystal packing (Figure 9).

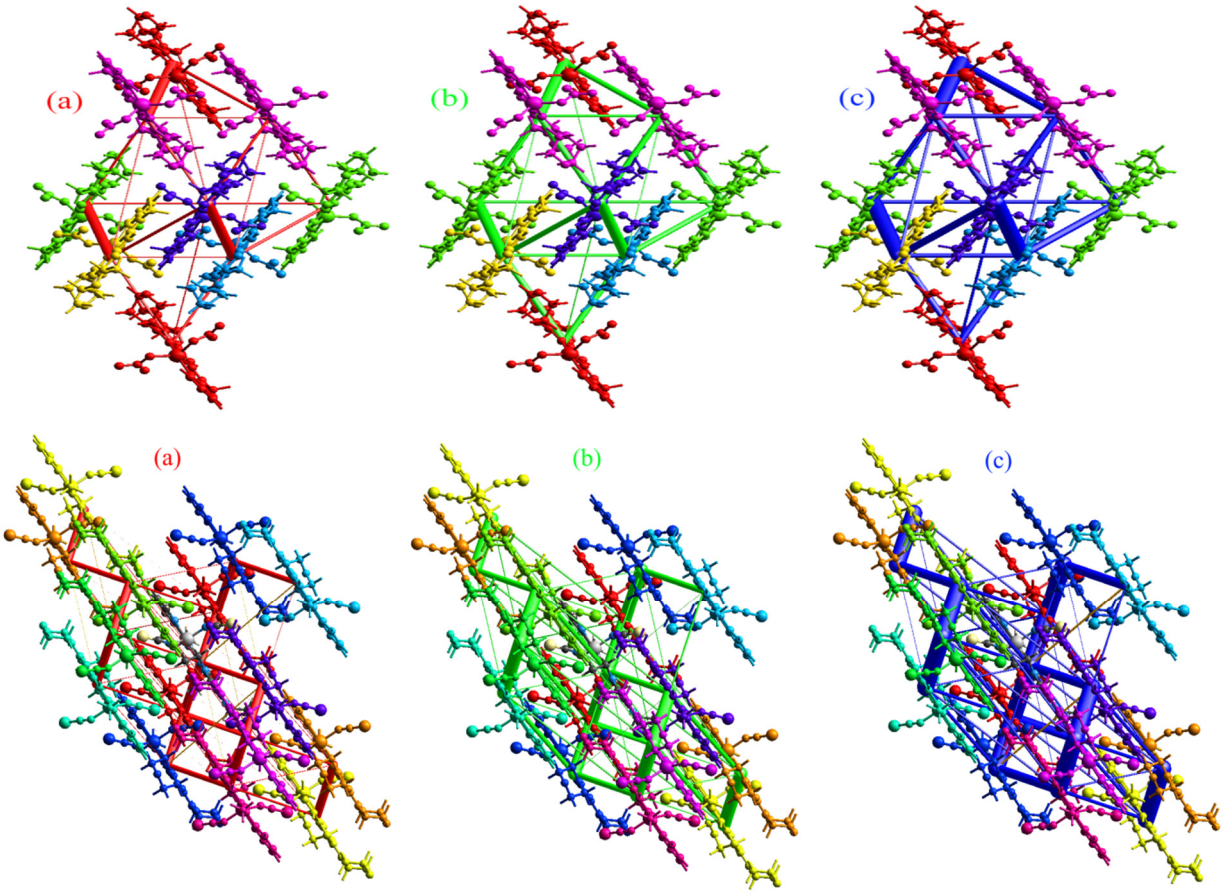


**Figure 9.** The EFW diagram illustrating the $E_{ele}$ (**a**), $E_{dis}$ (**b**), and $E_{tot}$ (**c**) for **1** (**upper**) and **2** (**lower**). The cylinder thicknesses indicated the relative strength of interactions between molecules.

### *2.6. NBO Charge Analysis*

For the two studied Zn(II) complexes, the divalent central metal ion is coordinated with one neutrally charged tridentate ligand and two mononegative species. The formal charges of these species in the isolated state are +2, 0, and −1, respectively. As a consequence of the metal–ligand Lewis acid–Lewis base interactions, the formal charges of these species are altered (Table 7). The two nitrate anions have comparable net charges of −0.764 and

−0.778 e, indicating negative charge transferences of 0.236 and 0.222 e to Zn(II), respectively. The corresponding values for the $NCS^-$ groups in complex **2** are 0.247 and 0.242 e. It seems that both anionic ligands transferred a similar amount of electron density to the central metal ion. Also, the neutral ligand **L** compensated the charge of Zn(II) by 0.325 and 0.365 e for complexes **1** and **2**, respectively. As a result, the charges of the Zn(II) are changed to 1.217 and 1.145 e, respectively.

**Table 7.** Charge analysis for the different species in complexes **1** and **2**.

| Species | Charge | Species | Charge |
|---|---|---|---|
| **1** | | **2** | |
| Ligand | 0.325 | Ligand | 0.365 |
| Zn1 | 1.217 | Zn1 | 1.145 |
| $NO_3^{-\,a}$ | −0.764 | $NCS^{-\,a}$ | −0.753 |
| $NO_3^{-\,b}$ | −0.778 | $NCS^{-\,b}$ | −0.758 |

Lower [a] and higher [b] atom numbering.

### *2.7. NBO Analysis*

Analysis of NBOs for the Zn-N and Zn-O interactions shed light on their relative strength and also on the nature of orbitals included in these interactions. The donor and acceptor NBOs included in the three Zn-N coordination interactions with the organic ligand are shown in Figure 10. It is clearly seen that the acceptor LP*(6) NBO of Zn1 is included in significant interactions with the donor NBO of the N-atoms (LP(1)N1, LP(1)N2, and LP(1)N4). Their interaction energies are calculated to be 27.48, 36.39, and 41.27 kcal/mol, respectively. In addition, each of these NBOs is also included in strong interactions with LP*(9), LP*(8), and LP*(9), respectively. Their $E_{int}$ values are 34.53, 32.97, and 29.10 kcal/mol, respectively (Table S3; Supplementary Data). For complex **2**, the NBOs included in the Zn-N donor–acceptor interactions with the organic ligand are almost the same.

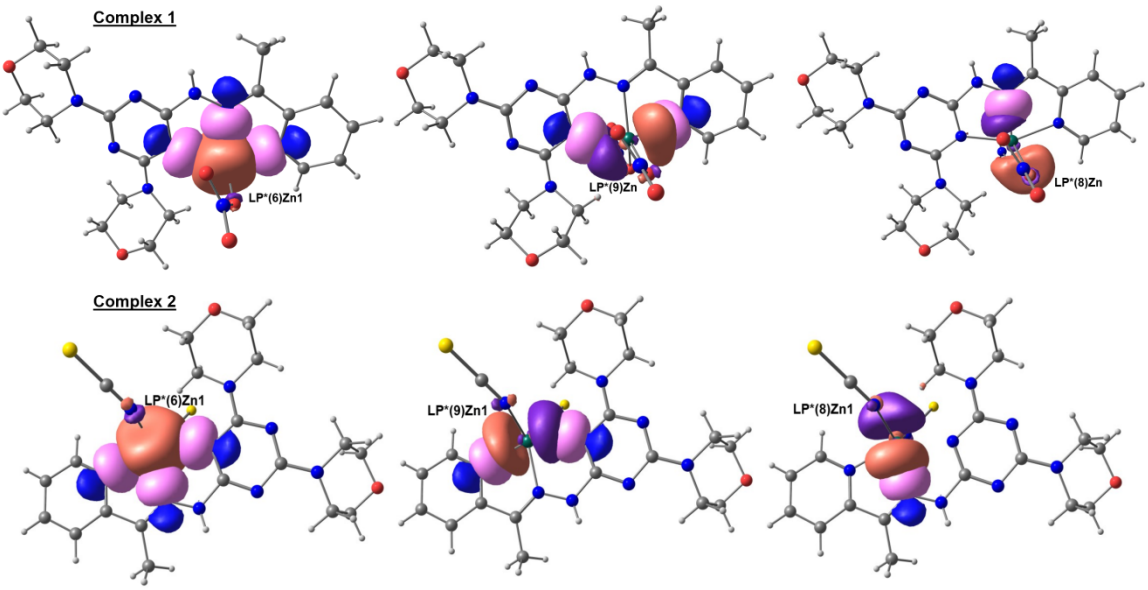


**Figure 10.** The NBOs involved in the Zn-N coordination interactions in **1** and **2**. The acceptor LP*(6) NBO is mainly s-orbital while the LP*(8) and LP*(9) have mixed p- and d-orbital characters. All donor NBOs have a mainly p-orbital character.

In addition, there is one strong and one weak Zn-O interaction for each coordinated $NO_3^-$ group. It is clearly evident from the NBO calculations that the Zn1-O3 and Zn1-O6 coordination interactions have a larger number of donor–acceptor NBO interactions

compared to the respective Zn1···O4 and Zn1···O7 ones. Also, the $E_{int}$ values of the formers are generally higher than the latter ones. For example, the LP(2)O3→LP*(6)Zn1 and LP(2)O6→LP*(6)Zn1 interactions have the highest interaction energies of 40.64 and 40.42 kcal/mol, respectively, which are higher than any of the donor–acceptor interactions included in the Zn1···O4 and Zn1···O7 interactions (Table 8 and Figure 11). Hence, the NBO analysis confirmed, with no doubt, the monodentate coordination behavior of both nitrate groups in **1**.

**Table 8.** The occupancy of Zn1 acceptor NBOs in complexes **1** and **2**.

| Acceptor NBO | 1 | 2 |
|---|---|---|
| LP*(6) | 0.324 | 0.342 |
| LP*(7) | 0.156 | 0.200 |
| LP*(8) | 0.148 | 0.168 |
| LP*(9) | 0.141 | 0.151 |

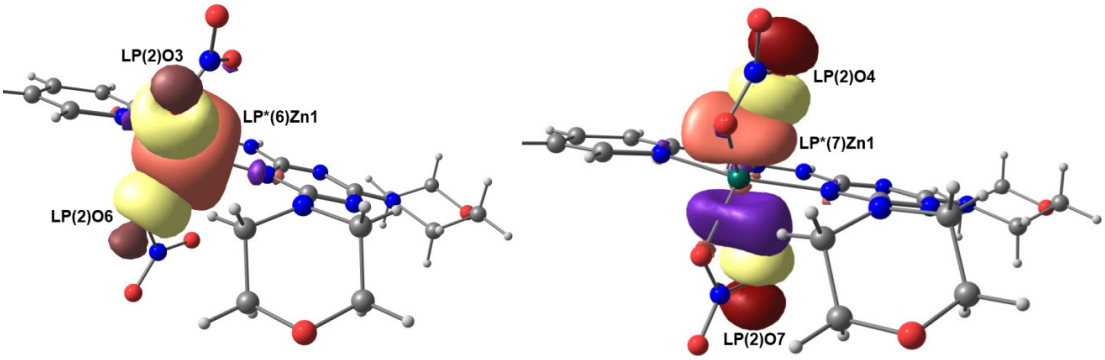


**Figure 11.** The donor and acceptor NBOs included in the Zn-O coordination interactions in **1**.

For complex **2**, the two most significant orbital interactions involved in the Zn-NCS bonds are presented in Figure 12. The LP(1)N→LP*(6)/LP*(7)Zn interactions have $E_{int}$ values of 71.84 and 63.84 kcal/mol, respectively, for the Zn1-N1 bond and 74.15 and 53.49 kcal/mol for Zn1-N2, respectively. The net $E_{int}$ values for the Zn1-N1 and Zn1-N2 bonds are 140.04 and 145.06 kcal/mol, respectively. The close interaction energies for both Zn-NCS bonds agreed very well with the close Zn1-N1 and Zn1-N2 distances.

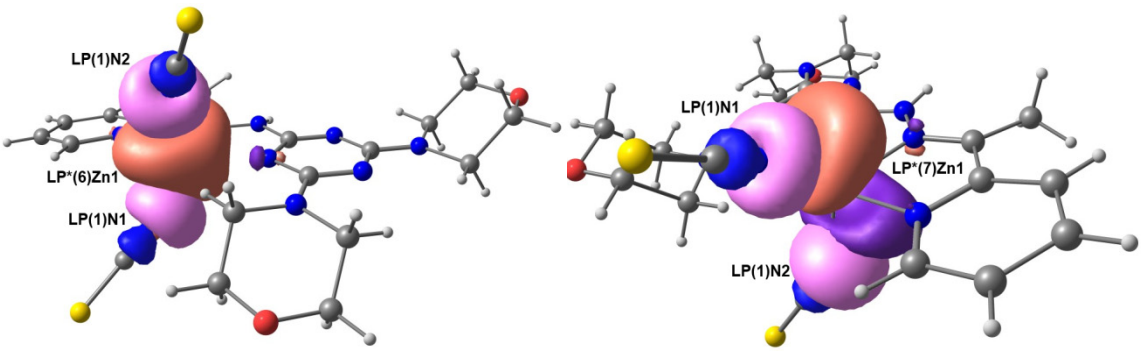


**Figure 12.** The donor and acceptor NBOs included in the Zn-NCS coordination interactions in **2**.

In Table 8, the occupancy of the different LP* NBOs of Zn1 in both complexes is depicted while the isolated Zn(II) ion has empty LP* NBOs. The results shown in this table indicated the partial occupancy of these orbitals as a consequence of the donor–acceptor interactions that occurred between the donor atoms from the ligand groups as the Lewis base with Zn(II) NBOs as the Lewis acid. The LP*(6) of Zn1 has the highest occupancies of 0.3236 and 0.3415 e for complexes **1** and **2**, respectively (Table 8). In this regard, the

electronic configuration of Zn1 is [core] $4S^{0.32}$ $3d^{9.98}$ $4p^{0.45}$ $4d^{0.02}$ $5p^{0.01}$ for **1** and [core] $4S^{0.34}$ $3d^{9.97}$ $4p^{0.53}$ $4d^{0.02}$ for **2**.

### 2.8. Antimicrobial Activity

In the light of the interesting biological activity of Zn(II) complexes for antimicrobial applications [12–17], the inhibition zone diameters (IZDs) and minimum inhibitory concentrations (MICs) for complexes **1** and **2** were determined against some infectious microbes (Table 9). Both complexes have wide-spectrum action against all the studied bacteria except *E.coli* while the free ligand showed no antibacterial activity [34]. The IZDs for the two Zn(II) complexes against bacteria and fungi range from 14 to 20 and 9 to 10 mm, respectively. In addition, the MICs range from 78 to 625 and 312 to 625 µg/mL, respectively. The best antibacterial action is found for complexes **1** and **2** against *P.vulgaris* where the IZDs are 18 and 20 mm, respectively. In addition, MICs are found to be 156 and 78 µg/mL, respectively. Hence, **2** slightly outperformed **1** as an antibacterial agent against *P.vulgaris*. It is interesting that the activity of complex **2** against *P.vulgaris* is comparable to gentamycin as a positive control (25 mm). Also, both Zn(II) complexes have good antibacterial activity against the gram-positive bacteria *S. aureus* and *B. subtilis* where the sizes of inhibition zones are in the range of 14–16 mm while the MICs range from 312 to 625 µg/mL. Regarding antifungal activity, both Zn(II) complexes are active against *C. albicans* while **1** is active against *A. fumigatus* but **2** is not (Table 9). As a result, the efficiency of Zn(II) complexes as antimicrobial agents against gram-positive bacteria and both fungal species are considered moderate compared to gentamycin and ketoconazole as positive controls, respectively.

**Table 9.** Antimicrobial activity (IZD; mm and MIC; µg/mL) for **1** and **2** compared to the structurally related complexes [a].

| Microorganism | L [a] | $[ZnL(ONO_2)_2]$; 1 | $[ZnL(NCS)_2]$; 2 | $[Mn(L)Cl_2]$ [a] | $[Cu(L)Cl_2]*H_2O$ [a] | Control |
|---|---|---|---|---|---|---|
| *S. aureus* | NA [b] (ND) [c] | 14(625) | 15(625) | 11(2500) | 18(625) | 24(78) [d] |
| *B. subtilis* | NA [b] (ND) [c] | 15(625) | 16(312) | 19(312) | 20(312) | 26(39) [d] |
| *E.coli* | NA [b] (ND) [c] | NA [b] (ND) [c] | NA [b] (ND) [c] | 10(2500) | NA(ND) | 30(10) [d] |
| *P.vulgaris* | NA [b] (ND) [c] | 18(156) | 20(78) | 12(1250) | 14(1250) | 25(5) [d] |
| *A. fumigatus* | NA [b] (ND) [c] | 10(625) | NA [b] (ND) [c] | NA [b] (ND) [c] | NA [b] (ND) [c] | 17(5) [e] |
| *C. albicans* | NA [b] (ND) [c] | 9(625) | 10(312) | 8(5000) | NA [b] (ND) [c] | 20(5) [e] |

[a] [34], [b] NA: No activity, [c] ND: (Not determined), [d] Gentamycin; [e] Ketoconazole.

For the structurally similar penta-coordinated metal (Mn(II) and Cu(II)) complexes of **L**, the antimicrobial activity showed wide variations depending on the metal ion and the nature of other coordinating ligand groups [34]. It is interesting that both Zn(II) complexes are the best acting as antifungal agents against the infectious *C. albicans* while the dichloro Mn(II) complex showed weak activity (IZD = 8 mm). In contrast, both the free **L** and the dichloro Cu(II) complex are inactive against the same fungus. Also, the Zn(II) complex **1** is active against *A. fumigatus* while the rest of the metal(II) complexes of the same ligand showed no activity against this infectious fungus. Regarding the antibacterial activity, the Zn(II) complex **2** is the best acting against *P.vulgaris* in comparison with the Mn(II) and Cu(II) complexes, which have inhibition zone diameters of 12 and 14 mm, respectively.

### 2.9. Cytotoxic Activity

Using the MTT assay, the in vitro cytotoxic effects of **1**, **2**, and **L** were evaluated versus HCT-116 and A-549 cancerous cells (ATCC, Rockville, MD). In addition, their safety profile was determined against human lung fibroblast normal cells (WI-38). The results indicated that **1**, **2**, and **L** have diverse inhibition behaviors against the tested cell lines (Table 10). The low $IC_{50}$ value for a tested compound indicates its strong effect on the harmful cancer cells. Hence, the cytotoxic activity of **1** is more than **2** against both cancerous cell lines. The $IC_{50}$ values of **1** are 29.53 ± 1.24 and 35.55 ± 1.69 µg/mL, respectively, while they are

41.25 ± 2.91 and 55.05 ± 2.87 μg/mL, respectively, for **2**. Hence, complex **1** has almost twice the cytotoxic efficiency against both cell lines compared to **2**. For the free **L**, the $IC_{50}$ values are found to be higher compared to their Zn(II) complexes. The organic chelate has $IC_{50}$ values of 59.85 ± 2.92 and 55.84 ± 2.74 μg/mL towards HCT-116 and A-549 cells, respectively [34]. As a result, the cytotoxic efficiency of the Zn(II) complexes is found to be better than the free ligand. Examining the effect of the studied compounds on normal WI-38 cell lines enabled us to judge whether these compounds could harm the normal cells or not and to what extent. In this regard, the selectivity index of the studied compounds is calculated. Regarding safety on normal cells, the selectivity index values (SI) for **1**, **2**, and **L** are higher than unity, confirming their safety of use as anticancer agents.

**Table 10.** Cytotoxicity of **1**, **2**, and **L** against HCT-116, A-549, and WI-38 cells and their selectivity indices (SI) utilizing MTT assay. Further details are given in Tables S4–S10 and Figures S6–S8 (Supplementary Data).

| Compound | HCT-116 | SI | A-549 | SI | WI-38 |
|---|---|---|---|---|---|
| **L** | 59.85 ± 2.92 [a] | 5.4 | 55.84 ± 2.74 [a] | 4.5 | 104.01 ± 3.61 |
| **[ZnL(ONO$_2$)$_2$]** | 29.53 ± 1.24 | 1.9 | 35.55 ± 1.69 | 1.6 | 55.95 ± 1.86 |
| **[ZnL(NCS)$_2$]** | 41.25 ± 2.91 | 1.5 | 55.05 ± 2.87 | 1.1 | 61.57 ± 2.17 |

[a] [34].

In comparison with the Mn(II) and Cu(II) complexes of **L**, the cytotoxic activity of these complexes is better than both Zn(II) complexes against the HCT-116 cell line [34]. Also, the Cu(II) complex has better cytotoxic activity (21.64±1.23 μg/mL) against the A-549 cell line than both Zn(II) complexes. In contrast, the Mn(II) complex is less potent (60.64 ± 3.08 μg/mL) as an anticancer agent than any of the two Zn(II) complexes against the A-549 cell line. In comparison with the common drug *cis*-platin, **1**, **2**, and **L** have lower cytotoxic activity against both cancerous cell lines ($IC_{50}$ = 8.4 ± 0.8 [52] and 19.3 ± 0.8 μg/mL [53], respectively).

## 3. Materials and Methods

### *3.1. Chemicals and Instruments*

All details for chemicals, solvents, and instruments are depicted in Supplementary Data.

### *3.2. Syntheses*

#### 3.2.1. Synthesis of [ZnL(ONO$_2$)$_2$]; **1**

Complex **1** was synthesized by combining $Zn(NO_3)_2{\cdot}6H_2O$ (0.2 mmol in 10 mL dist. $H_2O$) with **L** (0.2 mmol in 10 mL EtOH). After eight days, colorless crystals were formed and collected by filtration.

**[ZnL(ONO$_2$)$_2$]:** Yield: 85%; FTIR (KBr, cm$^{-1}$): 3224, 2969, 2904, 2854, 1579, 1513, 1265, 1391 (Figure S1; Supplementary Data). $C_{18}H_{24}N_{10}O_8Zn$: C, 37.68; H, 4.22; N, 24.41; Zn, 11.40%. Found: C, 37.43; H, 4.18; N, 24.29; Zn, 11.31%. $^1$H NMR (DMSO-$d_6$): (Figure S3; Supplementary Data) δ 9.72 (s, 1H, NH), 8.53 (brs, 1H, CHar), 8.06 (s, 1H, CHar), 7.78 (brs, 1H, CHar), 7.31 (brs, 1H, CHar), 3.71 (brs, 8H, 2 $CH_2$-O-$CH_2$), 3.59 (brs, 8H, 2 $CH_2$-N-$CH_2$), 2.33 (s, 3H, $CH_3$) ppm.

#### 3.2.2. Synthesis of [ZnL(NCS)$_2$]; **2**

Complex **2** was synthesized by mixing $Zn(ClO_4)_2{\cdot}6H_2O$ (0.2 mmol in 10 mL dist. $H_2O$) with **L** (0.2 mmol in 10 mL EtOH). To the resulting clear solution, 1 mL of saturated aqueous $NH_4SCN$ solution was added followed by reflux for 30 min then filtration. After ten days, colorless crystals were collected from the solution by filtration.

**[ZnL(NCS)$_2$]:** Yield: 88%; FTIR (KBr, cm$^{-1}$): 3187, 2963, 2908, 2857, 2084, 2047, 1588, 1502, 1256 (Figure S2; Supplementary Data). $C_{20}H_{24}N_{10}O_2S_2Zn$: C, 42.44; H, 4.27; N, 24.75; Zn, 11.55%. Found: C, 42.30; H, 4.22; N, 24.61; Zn, 11.40%.

### 3.3. X-ray Structure Determinations

The crystal structures of **1** and **2** were solved and refined as described in detail in Supplementary Data [54–57] and a summary of crystal data is given in Table 1.

### 3.4. Hirshfeld Analysis

Hirshfeld analysis [58] was conducted using the Crystal Explorer Ver. 21.5 program [59].

### 3.5. Computational Details

NBO analysis was performed using Gaussian 09 software [60] while the Chemcraft program [61] was used to construct the natural orbitals. The ωB97XD method employing 6–31G(d,p) basis sets for non-metal atoms and cc-pVTZ-PP for Zn [62] were used.

### 3.6. Biological Studies

The protocols for examining the cytotoxic activity [63] and antimicrobial efficacy [64] are outlined in Methods S1 and S2 (Supplementary Data).

## 4. Conclusions

Two new highly distorted penta-coordinated complexes, $[ZnL(ONO_2)_2]$ (**1**) and $[ZnL(NCS)_2]$ (**2**), with the *s*-triazine derivative (**L**) acting as a tridentate ligand, were synthesized and their structural, antimicrobial, and cytotoxic characteristics were explored. The free ligand (**L**) is a *NNN*-chelate from the pyridine, hydrazone, and *s*-triazine moieties, where the Zn-N of hydrazone is the shortest bond length while the Zn-N of *s*-triazine is the longest in both complexes. The $ZnN_3O_2$ and $ZnN_5$ coordination spheres have distorted square pyramidal configurations around Zn(II) in both complexes. Their supramolecular structure aspects were investigated using Hirshfeld surface analysis. The energy framework topology analysis indicated the importance of the dispersion energy term for the intermolecular interactions that occurred among the complex molecules, where total interaction energies of −317.8 and −353.5 kJ/mol were predicted for **1** and **2**, respectively. NBO analyses were used to predict the net charges of the ligand groups and metal ions as a consequence of the donor–acceptor interactions among them. In addition, the orbital–orbital interactions included in the Zn-O, Zn-N, and Zn-S interactions were described on the same basis. Complex **1** is a more potent anticancer agent than **2** against the HCT-116 and A-549 cell lines (SI >1). In contrast, the free **L** has higher $IC_{50}$ values, indicating the better cytotoxic properties of Zn(II) complexes compared to **L**. Also, both complexes have broad-spectrum antimicrobial activity. The best antibacterial action is found for complexes **1** and **2** against *P.vulgaris,* and are found to be comparable to gentamycin as a positive control. In addition, the antifungal activity of both Zn(II) complexes is better than other metal(II) analogs.

**Supplementary Materials:** The following supporting information can be downloaded at: https://www.mdpi.com/article/10.3390/inorganics12070176/s1. Experimental details; Figure S1. The FTIR spectra of **L** (upper) and $[ZnL(ONO_2)_2]$; **1** (lower); Figure S2. The FTIR spectra of $[ZnL(NCS)_2]$; **2**; Figure S3. The $^1$HNMR spectra of $[ZnL(ONO_2)_2]$; **1**; Figure S4. Shape index and curvedness maps for **1**; Figure S5. Shape index and curvedness maps for **2**; Figure S6. Visualization of molecular interactions within a cluster with a radius of 3.8 Å between the central molecule under investigation and its neighboring molecules, for **1**; (**A**) and **2**; (**B**); Figure S7. MTT assay of **1**, **2**, and their ligand **L** against WI-38 normal cells; Figure S8. MTT assay of **1** and **2** against HCT-116 cancerous cells; Figure S9. MTT assay of **1** and **2** against A-549 cancerous cells; Table S1. Different interaction energies[a] of the molecular pairs in kJ/mol for **1**; Table S2. Different interaction energies[a] of the molecular pairs in kJ/mol for **2**; Table S3. The NBO analysis for the Zn-N and Zn-O interactions in complexes **1** and **2**; Table S4. Evaluation of cytotoxicity against the WI-38 cell line for **L**; Table S5. Evaluation of cytotoxicity against the WI-38 cell line for **1**; Table S6. Evaluation of cytotoxicity against the WI-38 cell line for **2**; Table S7. Evaluation of cytotoxic activity against the HCT-116 cell line for **1**; Table S8. Evaluation of cytotoxic activity against the HCT-116 cell line for **2**; Table S9. Evaluation of cytotoxic activity against the A-549 cell line for **1**; Table S10. Evaluation of cytotoxic activity against the A-549 cell line for **2**; Method S1. Evaluation of

cytotoxic activity; Method S2. Evaluation of antimicrobial activity; Method S3. Energy framework analysis protocol.

**Author Contributions:** Conceptualization, M.A.M.A.-Y., A.Y. and S.M.S.; methodology, M.H. (MennaAllah Hassan) and A.Y.; software, M.H. (Matti Haukka), R.T., A.Y. and S.M.S.; validation, A.E.-F., A.Y. and A.B.; formal analysis, M.H. (MennaAllah Hassan), M.H. (Matti Haukka), R.T. and A.Y.; investigation, all; resources, A.Y., A.E.-F., A.B. and S.M.S.; data curation, M.H. (MennaAllah Hassan) and A.Y.; writing—original draft preparation, all; writing—review and editing, all; supervision, M.A.M.A.-Y., A.Y. and S.M.S.; funding acquisition, A.B. All authors have read and agreed to the published version of the manuscript.

**Funding:** The authors would like to extend their sincere appreciation to the Researchers Supporting Project (RSP2024R64), King Saud University, Riyadh, Saudi Arabia.

**Data Availability Statement:** The original contributions presented in the study are included in the article and Supplementary Materials, further inquiries can be directed to the corresponding authors.

**Acknowledgments:** The authors would like to extend their sincere appreciation to the Researchers Supporting Project (RSP2024R64), King Saud University, Riyadh, Saudi Arabia.

**Conflicts of Interest:** The authors declare no conflicts of interest.

## References

1. Pellei, M.; Del Bello, F.; Porchia, M.; Santini, C. Zinc coordination complexes as anticancer agents. *Coord. Chem. Rev.* **2021**, *445*, 214088. [CrossRef]
2. Vallee, B.L.; Auld, D.S. Zinc coordination, function, and structure of zinc enzymes and other proteins. *Biochemistry* **1990**, *29*, 5647–5659. [CrossRef]
3. Vallee, B.L.; Auld, D.S. Active-site zinc ligands and activated $H_2O$ of zinc enzymes. *Proc. Nat. Acad. Sci. USA* **1990**, *87*, 220–224. [CrossRef] [PubMed]
4. Lipscomb, W.N.; Sträter, N. Recent advances in zinc enzymology. *Chem. Rev.* **1996**, *96*, 2375–2434. [CrossRef] [PubMed]
5. Andreini, C.; Bertini, I. A bioinformatics view of zinc enzymes. *J. Inorg. Biochem.* **2012**, *111*, 150–156. [CrossRef]
6. Costello, L.C.; Fenselau, C.C.; Franklin, R.B. Evidence for operation of the direct zinc ligand exchange mechanism for trafficking, transport, and reactivity of zinc in mammalian cells. *J. Inorg. Biochem.* **2011**, *105*, 589–599. [CrossRef] [PubMed]
7. Federico, A.; Iodice, P.; Federico, P.; Del Rio, A.; Mellone, M.; Catalano, G. Effects of selenium and zinc supplementation on nutritional status in patients with cancer of digestive tract. *Eur. J. Clin. Nutr.* **2001**, *55*, 293–297. [CrossRef]
8. Prasad, A.S.; Beck, F.W.; Doerr, T.D.; Shamsa, F.H.; Penny, H.S.; Marks, S.C.; Kaplan, J.; Kucuk, O.; Mathog, R.H. Nutritional and zinc status of head and neck cancer patients: An interpretive review. *J. Am. Coll. Nutr.* **1998**, *17*, 409–418. [CrossRef] [PubMed]
9. d'Angelo, J.; Morgant, G.; Ghermani, N.E.; Desmaële, D.; Fraisse, B.; Bonhomme, F.; Dichi, E.; Sghaier, M.; Li, Y.; Journaux, Y. Crystal structures and physico-chemical properties of Zn(II) and Co(II) tetraaqua (3-nitro-4-hydroxybenzoato) complexes: Their anticonvulsant activities as well as related (5-nitrosalicylato)–metal complexes. *Polyhedron* **2008**, *27*, 537–546. [CrossRef]
10. Sakurai, H.; Kojima, Y.; Yoshikawa, Y.; Kawabe, K.; Yasui, H. Antidiabetic vanadium(IV) and zinc(II) complexes. *Coord. Chem. Rev.* **2002**, *226*, 187–198. [CrossRef]
11. Zhou, Q.; Hambley, T.W.; Kennedy, B.J.; Lay, P.A.; Turner, P.; Warwick, B.; Biffin, J.R.; Regtop, H.L. Syntheses and characterization of anti-inflammatory dinuclear and mononuclear zinc indomethacin complexes. Crystal structures of $[Zn_2(\text{indomethacin})_4(L)_2]$(L = *N*,*N*-dimethylacetamide,pyridine,1-methyl-2-pyrrolidinone) and $[Zn(\text{indomethacin})_2(L_1)_2]$($L_1$ = ethanol, methanol). *Inorg. Chem.* **2000**, *39*, 3742–3748. [PubMed]
12. Kasuga, N.C.; Sekino, K.; Ishikawa, M.; Honda, A.; Yokoyama, M.; Nakano, S.; Shimada, N.; Koumo, C.; Nomiya, K. Synthesis, structural characterization and antimicrobial activities of 12 zinc(II) complexes with four thiosemicarbazone and two semicarbazone ligands. *J. Inorg. Biochem.* **2003**, *96*, 298–310. [CrossRef] [PubMed]
13. Li, Z.Q.; Wu, F.J.; Gong, Y.; Hu, C.W.; Zhang, Y.H.; Gan, M.Y. Synthesis, characterization and activity against staphylococcus of metal(II)-gatifloxacin complexes. *Chin. J. Chem.* **2007**, *25*, 1809–1814. [CrossRef]
14. Chen, Z.-F.; Xiong, R.-G.; Zhang, J.; Chen, X.-T.; Xue, Z.-L.; You, X.-Z. 2D molecular square grid with strong blue fluorescent emission: A complex of norfloxacin with zinc(II). *Inorg. Chem.* **2001**, *40*, 4075–4077. [CrossRef]
15. Lopez-Gresa, M.; Ortiz, R.; Perelló, L.; Latorre, J.; Liu-Gonzalez, M.; Garcıa-Granda, S.; Perez-Priede, M.; Canton, E. Interactions of metal ions with two quinolone antimicrobial agents (cinoxacin and ciprofloxacin): Spectroscopic and X-ray structural characterization. Antibacterial studies. *J. Inorg. Biochem.* **2002**, *92*, 65–74. [CrossRef]
16. Xiao, D.R.; Wang, E.B.; An, H.Y.; Su, Z.M.; Li, Y.G.; Gao, L.; Sun, C.Y.; Xu, L. Rationally designed, polymeric, extended metal–ciprofloxacin complexes. *Chem. A Eur. J.* **2005**, *11*, 6673–6686. [CrossRef]
17. Tarushi, A.; Lafazanis, K.; Kljun, J.; Turel, I.; Pantazaki, A.A.; Psomas, G.; Kessissoglou, D.P. First-and second-generation quinolone antibacterial drugs interacting with zinc(II): Structure and biological perspectives. *J. Inorg. Biochem.* **2013**, *121*, 53–65. [CrossRef] [PubMed]

18. Tarushi, A.; Karaflou, Z.; Kljun, J.; Turel, I.; Psomas, G.; Papadopoulos, A.N.; Kessissoglou, D.P. Antioxidant capacity and DNA-interaction studies of zinc complexes with a non-steroidal anti-inflammatory drug, mefenamic acid. *J. Inorg. Biochem.* **2014**, *128*, 85–96. [CrossRef]
19. Tarushi, A.; Totta, X.; Papadopoulos, A.; Kljun, J.; Turel, I.; Kessissoglou, D.P.; Psomas, G. Antioxidant activity and interaction with DNA and albumins of zinc–tolfenamato complexes. Crystal structure of [Zn(tolfenamato)$_2$(2,2′-dipyridylketoneoxime)$_2$]. *Eur. J. Med. Chem.* **2014**, *74*, 187–198. [CrossRef]
20. Kovala-Demertzi, D.; Yadav, P.N.; Wiecek, J.; Skoulika, S.; Varadinova, T.; Demertzis, M.A. Zinc(II) complexes derived from pyridine-2-carbaldehyde thiosemicarbazone and (1*E*)-1-pyridin-2-ylethan-1-one thiosemicarbazone. Synthesis, crystal structures and antiproliferative activity of zinc(II) complexes. *J. Inorg. Biochem.* **2006**, *100*, 1558–1567. [CrossRef]
21. Belicchi Ferrari, M.; Bisceglie, F.; Pelosi, G.; Tarasconi, P.; Albertini, R.; Pinelli, S. New methyl pyruvate thiosemicarbazones and their copper and zinc complexes: Synthesis, characterization, X-ray structures and biological activity. *J. Inorg. Biochem.* **2001**, *87*, 137–147. [CrossRef]
22. Trávníček, Z.; Kryštof, V.; Šipl, M. Zinc(II) complexes with potent cyclin-dependent kinase inhibitors derived from 6-benzylaminopurine: Synthesis, characterization, X-ray structures and biological activity. *J. Inorg. Biochem.* **2006**, *100*, 214–225. [CrossRef] [PubMed]
23. Di Vaira, M.; Bazzicalupi, C.; Orioli, P.; Messori, L.; Bruni, B.; Zatta, P. Clioquinol, a Drug for Alzheimer's disease specifically interfering with brain metal metabolism: structural characterization of its zinc(II) and copper(II) complexes. *Inorg. Chem.* **2004**, *43*, 3795–3797. [CrossRef] [PubMed]
24. Ali, M.M.; Frei, E.; Straub, J.; Breuer, A.; Wiessler, M. Induction of metallothionein by zinc protects from daunorubicin toxicity in rats. *Toxicology* **2002**, *179*, 85–93. [CrossRef] [PubMed]
25. Klenke, B.; Barrett, M.P.; Brun, R.; Gilbert, I.H. Antiplasmodial activity of a series of 1,3,5-triazine-substituted polyamines. *J. Antimicrob. Chemother.* **2003**, *52*, 290–293. [CrossRef] [PubMed]
26. Srinivas, K.; Srinivas, U.; Bhanuprakash, K.; Harakishore, K.; Murthy, U.; Rao, V.J. Synthesis and antibacterial activity of various substituted *s*-triazines. *Eur. J. Med. Chem.* **2006**, *41*, 1240–1246. [CrossRef] [PubMed]
27. Mandal, S.; Bérubé, G.; Asselin, É.; Mohammad, I.; Richardson, V.J.; Gupta, A.; Pramanik, S.K.; Williams, A.L.; Mandal, S.K. A novel series of potent cytotoxic agents targeting G2/M phase of the cell cycle and demonstrating cell killing by apoptosis in human breast cancer cells. *Bioorg. Med. Chem. Lett.* **2007**, *17*, 4955–4960. [CrossRef] [PubMed]
28. Garaj, V.; Puccetti, L.; Fasolis, G.; Winum, J.-Y.; Montero, J.-L.; Scozzafava, A.; Vullo, D.; Innocenti, A.; Supuran, C.T. Carbonic anhydrase inhibitors: Novel sulfonamides incorporating 1,3,5-triazine moieties as inhibitors of the cytosolic and tumour-associated carbonic anhydrase isozymes I, II and IX. *Bioorg. Med. Chem. Lett.* **2005**, *15*, 3102–3108. [CrossRef] [PubMed]
29. Ma, S.; Zhou, H.-C. A metal− organic framework with entatic metal centers exhibiting high gas adsorption affinity. *J. Am. Chem. Soc.* **2006**, *128*, 11734–11735. [CrossRef]
30. Chae, H.K.; Kim, J.; Friedrichs, O.D.; O'Keeffe, M.; Yaghi, O.M. Design of frameworks with mixed triangular and octahedral building blocks exemplified by the structure of [$Zn_4O(TCA)_2$] having the pyrite topology. *Angew. Chem. Int. Ed.* **2003**, *42*, 3907–3909. [CrossRef]
31. Kepert, C.J.; Rosseinsky, M.J. Zeolite-like crystal structure of an empty microporous molecular framework. *Chem. Commun.* **1999**, *4*, 375–376. [CrossRef]
32. Wang, S.-N.; Xing, H.; Li, Y.-Z.; Bai, J.; Scheer, M.; Pan, Y.; You, X.-Z. Unprecedented interweaving of single-helical and unequal double-helical chains into chiral metal–organic open frameworks with multiwalled tubular structures. *Chem. Commun.* **2007**, *22*, 2293–2295. [CrossRef]
33. Soliman, S.M.; Elsilk, S.E.; El-Faham, A. Synthesis, structure and biological activity of zinc(II) pincer complexes with 2,4-*bis*(3,5-dimethyl-1*H*-pyrazol-1-yl)-6-methoxy-1,3,5-triazine. *Inorg. Chim. Acta* **2020**, *508*, 119627. [CrossRef]
34. Fathalla, E.M.; Abu-Youssef, M.A.; Sharaf, M.M.; El-Faham, A.; Barakat, A.; Badr, A.M.; Soliman, S.M.; Slawin, A.M.; Woollins, J.D. Synthesis, characterizations, antitumor and antimicrobial evaluations of novel Mn(II) and Cu(II) complexes with *NNN*-tridentate *s*-triazine-Schiff base ligand. *Inorg. Chim. Acta* **2023**, *555*, 121586. [CrossRef]
35. Fathalla, E.M.; Abu-Youssef, M.A.; Sharaf, M.M.; El-Faham, A.; Barakat, A.; Haukka, M.; Soliman, S.M. Synthesis, X-ray structure of two hexa-coordinated Ni(II) complexes with *s*-triazine hydrazine Schiff base ligand. *Inorganics* **2023**, *11*, 222. [CrossRef]
36. Addison, A.W.; Rao, T.N.; Reedijk, J.; van Rijn, J.; Verschoor, G.C. Synthesis, structure, and spectroscopic properties of copper(II) compounds containing nitrogen–sulphur donor ligands; the crystal and molecular structure of aqua [1,7-*bis*(*N*-methylbenzimidazol-2′-yl)-2,6-dithiaheptane]copper(II) perchlorate. *J. Chem. Soc. Dalton Trans.* **1984**, *7*, 1349–1356. [CrossRef]
37. Morozov, I.; Serezhkin, V.; Troyanov, S. Modes of coordination and stereochemistry of the $NO_3^-$ anions in inorganic nitrates. *Russ. Chem. Bull.* **2008**, *57*, 439–450. [CrossRef]
38. Kleywegt, G.J.; Wiesmeijer, W.G.; Van Driel, G.J.; Driessen, W.L.; Reedijk, J.; Noordik, J.H. Unidentate versus symmetrically and unsymmetrically bidentate nitrate co-ordination in pyrazole-containing chelates. The crystal and molecular structures of (nitrato-*O*)[tris(3,5-dimethylpyrazol-1-ylmethyl)amine]copper(II) nitrate,(nitrato-*O*,*O*′)[tris(3,5-dimethylpyrazol-1-ylmethyl)amine]nickel(II) nitrate, and (nitrato-*O*)(nitrato-*O*,*O*′)[tris(3,5-dimethylpyrazol-1-ylmethyl) amine]cadmium(II). *J. Chem. Soc. Dalton Trans.* **1985**, *10*, 2177–2184.
39. Janiak, C. A critical account on π–π stacking in metal complexes with aromatic nitrogen-containing ligands. *J. Chem. Soc. Dalton Trans.* **2000**, *21*, 3885–3896. [CrossRef]

40. Turner, M.J.; Thomas, S.P.; Shi, M.W.; Jayatilaka, D.; Spackman, M.A. Energy frameworks: Insights into interaction anisotropy and the mechanical properties of molecular crystals. *Chem. Commun.* **2015**, *51*, 3735–3738.
41. Bakheit, A.H.; Attwa, M.W.; Kadi, A.A.; Alkahtani, H.M. Structural Analysis and Reactivity Insights of (*E*)-Bromo-4-((4-((1-(4-chlorophenyl)ethylidene)amino)-5-phenyl-4H-1,2,4-triazol-3-yl)thio)-5-((2-isopropylcyclohexyl)oxy) Furan-2(5H)-one: A combined approach using single-crystal X-ray diffraction, Hirshfeld surface analysis, and conceptual density functional theory. *Crystals* **2023**, *13*, 1313. [CrossRef]
42. Turner, M.J.; Grabowsky, S.; Jayatilaka, D.; Spackman, M.A. Accurate and efficient model energies for exploring intermolecular interactions in molecular crystals. *J. Phys. Chem. Lett.* **2014**, *5*, 4249–4255. [CrossRef]
43. Hajji, M.; Mtiraoui, H.; Amiri, N.; Msaddek, M.; Guerfel, T. Crystallographic and first-principles density functional theory study on the structure, noncovalent interactions, and chemical reactivity of 1,5-benzodiazepin-2-ones derivatives. *Int. J. Quantum Chem.* **2019**, *119*, e26000. [CrossRef]
44. Abad, N.; Sallam, H.H.; Al-Ostoot, F.H.; Khamees, H.A.; Al-horaibi, S.A.; Khanum, S.A.; Madegowda, M.; El Hafi, M.; Mague, J.T.; Essassi, E.M. Synthesis, crystal structure, DFT calculations, Hirshfeld surface analysis, energy frameworks, molecular dynamics and docking studies of novel isoxazolequinoxaline derivative (IZQ) as anti-cancer drug. *J. Mol. Struct.* **2021**, *1232*, 130004. [CrossRef]
45. Edwards, A.J.; Mackenzie, C.F.; Spackman, P.R.; Jayatilaka, D.; Spackman, M.A. Intermolecular interactions in molecular crystals: What's in a name? *Faraday Discuss.* **2017**, *203*, 93–112. [CrossRef] [PubMed]
46. Mackenzie, C.F.; Spackman, P.R.; Jayatilaka, D.; Spackman, M.A. CrystalExplorer model energies and energy frameworks: Extension to metal coordination compounds, organic salts, solvates and open-shell systems. *IUCrJ* **2017**, *4*, 575–587. [CrossRef] [PubMed]
47. Wang, K.; He, X.; Rong, C.; Zhong, A.; Liu, S.; Zhao, D. On the origin and nature of internal methyl rotation barriers: An information-theoretic approach study. *Theor. Chem. Acc.* **2022**, *141*, 68. [CrossRef]
48. Zhong, A.; Chen, D.; Li, R. Revisiting the beryllium bonding interactions from energetic and wavefunction perspectives. *Chem. Phys. Lett.* **2015**, *633*, 265–272. [CrossRef]
49. Tan, S.L.; Jotani, M.M.; Tiekink, E.R. Utilizing Hirshfeld surface calculations, non-covalent interaction (NCI) plots and the calculation of interaction energies in the analysis of molecular packing. *Acta Crystallogr. E Crystallogr. Commun.* **2019**, *75*, 308–318. [CrossRef]
50. Sreenatha, N.; Chakravarthy, A.J.; Suchithra, B.; Lakshminarayana, B.; Hariprasad, S.; Ganesha, D. Crystal, spectral characterization, molecular docking, Hirshfeld computational studies and 3D-energy framework analysis of a novel puckered compound ($C_{14}H_{15}ClO$): 2-Chloro-3-phenyl-5,5-dimethylcyclohex-2-en-1-one. *J. Mol. Struct.* **2020**, *1210*, 127979. [CrossRef]
51. Guo, Z.A.; Xian, J.Y.; Rong, L.R.; Qin, H.; Jie, Z. Theoretical study of metal ion impact on geometric and electronic properties of terbutaline compounds. *Monatsh. Chem.* **2019**, *150*, 1355–1364. [CrossRef]
52. Kheiralla, Z.M.; Abo-Ghalia, H.H.; Elaasser, M.M.; Hemeda, M.F.; Ibrahim, S.Y. Endophyte Chaetomium, Potential Bioactivity: Pharmaceutical and Phytochemical Analyses. *Res. Sq.* **2023**. [CrossRef]
53. Gomha, S.M.; Muhammad, Z.A.; Abdel-aziz, M.R.; Abdel-aziz, H.M.; Gaber, H.M.; Elaasser, M.M. One-pot synthesis of new thiadiazolyl-pyridines as anticancer and antioxidant agents. *J. Heterocycl. Chem.* **2018**, *55*, 530–536. [CrossRef]
54. Rikagu Oxford Diffraction. *CrysAlisPro 1.171.43.100a*; Rikagu Oxford Diffraction Inc.: Yarnton, Oxfordshire, UK, 2023.
55. Sheldrick, G.M. *SHELXT*—Integrated space-group and crystal-structure determination. *Acta Cryst.* **2015**, *A71*, 3–8. [CrossRef] [PubMed]
56. Sheldrick, G.M. Crystal Structure Refinement with SHELXL. *Acta Cryst.* **2015**, *C71*, 3–8.
57. Dolomanov, O.V.; Bourhis, L.J.; Gildea, R.J.; Howard, J.A.K.; Puschmann, H.J. *OLEX2*: A complete structure solution, refinement and analysis program. *Appl. Cryst.* **2009**, *42*, 339–341. [CrossRef]
58. Turner, M.; McKinnon, J.; Wolff, S.; Grimwood, D.; Spackman, P.; Jayatilaka, D.; Spackman, M. *CrystalExplorer17*; University of Western Australia: Perth, Australia, 2017.
59. Spackman, M.A.; Jayatilaka, D. Hirshfeld surface analysis. *CrystEngComm* **2009**, *11*, 19–32. [CrossRef]
60. Frisch, M. *gaussian 09, Revision d. 01*; Gaussian. Inc.: Wallingford, CT, USA, 2009; Volume 201.
61. Andrienko, G. Chemcraft-Graphical Software for Visualization of Quantum Chemistry Computations. Version 1.8, Build 682. 2010. Available online: https://www.chemcraftprog.com (accessed on 22 July 2020).
62. Pritchard, B.P.; Altarawy, D.; Didier, B.; Gibson, T.D.; Windus, T.L. New basis set exchange: An open, up-to-date resource for the molecular sciences community. *J. Chem. Inf. Model.* **2019**, *59*, 4814–4820. [CrossRef]
63. Mosmann, T. Rapid colorimetric assay for cellular growth and survival: Application to proliferation and cytotoxicity assays. *J. Immunol. Methods* **1983**, *65*, 55–63. [CrossRef]
64. Lu, P.-L.; Liu, Y.-C.; Toh, H.-S.; Lee, Y.-L.; Liu, Y.-M.; Ho, C.-M.; Huang, C.-C.; Liu, C.-E.; Ko, W.-C.; Wang, J.-H. Epidemiology and antimicrobial susceptibility profiles of gram-negative bacteria causing urinary tract infections in the Asia-Pacific region: 2009–2010 results from the Study for Monitoring Antimicrobial Resistance Trends (SMART). *Int. J. Antimicrob. Agents* **2012**, *40*, S37–S43. [CrossRef]